

Superconducting properties of PEO coatings containing MgB₂ on niobium

S. Aliasghari^{1,2}, P. Skeldon², X. Zhou², R. Valizadeh¹, T. Junginger^{3,4}, G.B.G. Stenning⁵,
G. Burt^{3,4}

¹ ASTeC, STFC Daresbury Laboratory, Daresbury, Warrington, Cheshire WA4 4AD, UK.

² Corrosion and Protection Group, School of Materials, The University of Manchester, Manchester M13 9PL, UK.

³ Engineering Building, Lancaster University, Lancaster, LA1 4YW, UK.

⁴ Cockcroft Institute, Keckwick Ln, Daresbury, Warrington, WA4 4AD, UK.

⁵ ISIS, STFC Rutherford Appleton Laboratory, Didcot, OX11 0QX, UK

Abstract

A study has been carried out of superconductivity in coatings formed on niobium by plasma electrolytic oxidation (PEO) in electrolyte containing different concentrations of MgB_2 . From preliminary experiments, a suitable PEO condition was selected. The coatings were examined by analytical scanning electron microscopy and X-ray diffraction. Superconductivity was assessed using magnetic moment-field measurements. At 6 K, superconductivity of the niobium dominated, which revealed strong flux pinning and sudden release. The latter was more gradual following PEO, indicating pinning was a surface effect. Between the critical temperature of niobium (9.25 K) and MgB_2 (about 39 K), the diamagnetic behaviour of superconducting MgB_2 was present, with earlier flux penetration the closer the temperature to 39 K. The hysteresis loop indicated stronger flux pinning for lower temperatures, as expected for a superconductor.

Keywords: plasma electrolytic oxidation, coating, magnesium, boride, superconductivity

1. Introduction

A recent short communication of the present authors provided the first report of the possibility of forming superconducting coatings using plasma electrolytic oxidation (PEO) [1]. Superconductivity arose from MgB_2 particles incorporated from the electrolyte into a coating composed of niobium and silicon oxides. PEO coatings are formed at high voltages during anodic polarization of a suitable metal substrate, most commonly aluminium, magnesium and titanium, in a liquid, usually aqueous, electrolyte [2, 3]. A porous coating material containing nano- to micro-sized pores [4, 5] is generated at the locations of microdischarges, with lifetimes in the microsecond to millisecond range [6-8], on the substrate surface. The coating material, often oxide-based [9-11], is probably formed by a mixture of processes, involving anodic oxidation, thermal oxidation and plasma-chemical reactions under the high temperatures and pressures at the microdischarge sites. Species from both the substrate and the electrolyte are incorporated into the coating, including the possibility of incorporation of nanoparticles if present as an addition to the electrolyte [13-15]. Usually the coating thickness is determined by the time of the PEO treatment [9, 15], with thicknesses up to the order tens of microns being possible. The rapid heating and cooling of the coating material at microdischarge sites results

in coatings that generally contain both crystalline and amorphous components in proportions dependent upon the PEO conditions, e.g. electrolyte composition and electrical parameter (e.g. DC, AC, frequency, waveform). The formation of the coating is accompanied by significant generation of gas, including bubbles of oxygen, hydrogen and water vapour [3, 16].

In the previous study [1], the selected substrate was niobium, as it is of interest as a superconducting material (critical temperature 9.25 K) [17-18], and the applicability of PEO [19, 20]. Superconductivity was evident below 39 K, the critical temperature for MgB [21], owing to the presence of MgB₂ particles in the oxide coating [1]. Various other processes have been used to produce superconducting MgB₂ coatings e.g. pulsed laser deposition (PLD) [22], low pressure chemical vapour deposition (LPCVD) [23], molecular beam epitaxy (MBE) [24], hybrid physical chemical vapour deposition (HPCVD) [25], reactive evaporation [26], electroless [27], electrochemical synthesis [28], electrophoretic [29], sol-gel [30], and ion beam [31]. However, these techniques have some drawbacks, e.g. MgB₂ phase stability, contamination and oxidation, line-of-sight access, and use of reactive chemicals, vacuum, and high temperatures. PEO is an alternative process that has received little attention for such an application. Of potential advantage, PEO can be used to treat large components, does not rely on line-of-sight access to the surfaces on which the coating is to be deposited, uses non-toxic treatment baths and does not require use of vacuum systems or high temperatures.

The present work investigated the influence of the current waveform and treatment time on PEO coating formation on niobium, which was used to select treatment parameters for formation of coatings incorporating MgB₂ particles. PEO coatings containing MgB₂ are of possible interest for use in superconducting radio frequency (SRF) cavities for particle accelerators [32, 33]. For the preferred coating condition, the superconductivity properties of the coated substrate were investigated in the temperature range 6 to 45 K using magnetization-field measurements, not previously reported, made with a superconducting quantum interference device.

2. Experimental

2.1. Material and PEO conditions

Specimens were cut from 99.6% niobium sheet, of 2.0 mm thickness (ADVENT Research Materials Ltd.), ground to a 1200 SiC grade finish, degreased with acetone, rinsed with deionized water, dried in air at 40 °C and coated in lacquer (Stopper 45 MacDermid), leaving a working area of $\sim 1 \times 1 \text{ cm}^2$.

PEO was carried out for up to 2000 s at a constant rms current density of 500 mA cm^{-2} with a square wave using an ACS-FB power supply (ET System Electronic GmbH). The frequency was 50 Hz, with a duty cycle of 50%, and a negative to positive current ratio (i_n/i_p) in the range -1 to -1.27. The electrolyte consisted of reagent grade sodium silicate (10.5 g l^{-1} specific gravity 1.5), phosphoric acid (3 ml l^{-1}) and sodium hydroxide (2.8 g l^{-1}) in deionized water. As required, either 3 or 8 g l^{-1} of MgB_2 powder (99% purity-Alfa Aesar), which was first dispersed ultrasonically in 100 cm^3 of the electrolyte for 30 min, were added. The electrical parameters and base electrolyte were selected from previous work of the authors on PEO coating of titanium [34].

A double-walled glass cell contained 1 dm^3 of electrolyte, which was stirred using a magnetic stirrer. The electrolyte was kept at 25 °C by a flow of cold water through the cell wall. A $7.5 \times 15 \text{ cm}$ type 304 stainless steel plate was used as a counter electrode. Voltage–time responses were recorded employing LabView software with a sampling time of 20 ms.

Light emitted by discharges was collected using an optical emission spectroscope (USB4000 Ocean Optics), with an optical fibre immersed in the electrolyte, and located 10 mm from the specimen to optimize the collection. The optical fibre (ZFQ-9596, Ocean Optics) was of 1000 μm diameter, with a numerical aperture of 0.22 ± 0.22 . Emissions were recorded in the wavelength range 200–850 nm with a resolution of 1 nm.

2.2. Specimen examination

PEO-treated specimens were examined using a Zeiss Ultra 55 scanning electron microscope, equipped with energy dispersive X-ray (EDX) analysis facilities. Cross-sections were prepared using successive grades of SiC paper, followed by finishing with 1 μm diamond paste. Phase composition was investigated by X-ray diffraction (XRD), using a Philips X'Pert-MPD (PW 3040) instrument with copper $K\alpha$ radiation, a step size of 0.005° and a scan range from 5° to 85° (in 2θ).

2.3 SQUID measurements

All deposited niobium films were analyzed using a superconducting quantum interference device (SQUID), quantum design MPMS XL-7 to measure magnetic hysteresis loops in a dc magnetic field at 6 K. In application to SRF cavities, the magnetic field should be parallel to the surface. All samples were oriented as close to parallel to the plane of the magnetic field as was possible to achieve. The error in the sample alignment with the magnetic field was 1° (17 mrad). The sensitivity of the magnetic property measurement system (MPMS) system is 10^{-7} emu; however, in the reported experiments the noise level of the magnetic moment measurements was observed to be 10^{-4} emu at zero field.

3. Results and discussion

3.1 Voltage-time response

Figure 1(a) presents the voltage-time response for PEO of niobium for 2000 s in the MgB₂-free electrolyte with i_n/i_p of -1. The voltage increased in 7 s to 290 V as a barrier anodic film was formed. Earlier studies of anodic niobia barrier film growth show that the thickness increases in proportion to the increasing voltage at about 2.1 to 2.3 nm V⁻¹ [35, 36]. Sparks then initiated when the voltage reached the dielectric breakdown voltage (290 V) of the anodic film. The PEO stage of the process then commenced in the presence of sparking and gas evolution. The gas comprises hydrogen and oxygen generated electrochemically and also be thermal dissociation of water under radiolysis in the discharge channels [3, 16]. The electrolyte may also boil producing bubbles of water vapour on the coating surface that subsequently collapse as the water vapour condenses [3].

After sparking begins, the voltage remained steady until 200 s, increased to 325 V at 700 s, and then decreased to 150 V at 1200 s. The decline in voltage was accompanied by relatively small voltage fluctuations that gradually increased in magnitude. Thereafter, large fluctuations developed about a mean voltage of about 140 V. These occurred with decreasing frequency and magnitude up to the end of the treatment, with peak-to-trough voltage differences initially of about 120 V and finally about 100 V. The minimum voltages were about 85 V. During these large transients sparking was sporadic. Individual transients comprised a voltage drop that

occurred in 10 to 18 s, followed by a gradual recovery over an interval that ranged from about 40 to 80 s. The inability to support sustained dielectric breakdown at this stage of the process suggests that the barrier layer at the coating base was cyclically degraded, for instance due to stresses from coating growth and gas evolution causing detachment of the barrier layer from the substrate. This causes the voltage to decrease, followed by a recovery as the damage is healed.

The effect of changing i_n/i_p from -1 to -1.27 was negligible (see Fig. 1(b)). The differences between curves were within the limits of reproducibility. The negligible effect of changing i_n/i_p contrasts with PEO of aluminium or magnesium, when a transition to a so-called “soft” sparking regime occurs with increase of the negative current [37-40]. The onset of “soft sparking” has been suggested to be due to factors such as change of the pH and electric field at the metal/oxide interface [38], and to be influenced by the nature of the electrolyte cations [39]. Following PEO on the present specimens, a white coating was formed, which had a uniform appearance across the whole of the working area.

From the previous experiments, $i_n/i_p = -1$ and 720 s were chosen for carrying out PEO treatments in electrolytes containing 3 and 8 g l⁻¹ MgB₂. **The additions of MgB₂ particles led to an increase in the voltage during sparking by about 7 and 18 V, respectively** (Fig. 1(c)). Furthermore, addition of 8 g l⁻¹ MgB₂ particles led to a rapid voltage drop, by about 100 V, after 550 s, with the final voltage after 720 s being about 220 V. It is later shown that more MgB₂ was incorporated into the coating formed in the electrolyte containing 8 g l⁻¹ MgB₂ compared with the electrolyte containing 3 g l⁻¹. The decrease in voltage at the later stages of PEO with the higher concentration of MgB₂ indicates a less resistive coating, possibly due to MgB₂ particles reaching the barrier layer and disrupting its continuity on the niobium substrate. Current may then be preferentially diverted from oxidation of the niobium to electrochemical generation of oxygen and hydrogen on the particles at the niobium/coating interface under voltages below the dielectric breakdown voltage. The coatings formed in electrolytes containing particles were dark grey, similar to the colour of the MgB₂ powder.

3.2 Optical emission spectroscopy

Figure 2 displays the optical emission spectra recorded every 60 s during PEO in the MgB₂-free electrolyte for 600 s at $i_n/i_p = -1$. The use of the particle-free electrolyte was necessary

since additions of MgB₂ rendered the electrolyte opaque. Emissions were detected at 180 s from sodium (Na I 589.6 nm) and hydrogen (H_α 656.3nm) and niobium (Nb 306.96 nm); small peaks were also present due to hydrogen (H_β 486.1 nm) and silicon (Si I 288.1 nm). Sparking first occurred at the edges of the working area, then spread inwards to cover the whole working area by 240 s, when the emission intensities were highest. The emission from niobium gave a predominantly violet hue to the initial sparking. After 360 s, Na I was the main emission line, which resulted in an orange appearance of sparks. At 600 s, only a weak Na I peak was resolved as the number and intensity of sparks reduced.

3.3 Coating morphology and composition

The dependence of the coating thickness, determined from SEM of cross-sections, on PEO time at $i_p/i_n = -1$ is shown in Fig. 3. Between 240 to 720 s, the thickness increased linearly with time at a rate of 115 nm⁻¹ s up to a thickness of ≈60 μm. The rate then fell to an average of 30 nm s⁻¹ between 720 to 1800 s coinciding with the decreasing and fluctuating voltage observed in the voltage-time curve of Fig. 1.

A secondary electron micrograph of a cross-section of a coating formed in the absence of MgB₂ particles for 720 s at i_n/i_p of 1 reveals a variable coating thickness due to the presence of large nodules of coating material (Fig. 4(a)); the thickness mainly ranged from ≈50 to 70 μm. However, pores and channels are present throughout the coating, some channels penetrating to within a few microns from the niobium substrate. A thin barrier layer is present across the niobium surface with a thickness of about 1 μm. The accompanying EDS elemental maps (Figs. 4(b-d)) show the presence of oxygen and silicon in most regions, while niobium occurs mainly near to the substrate. Sodium and phosphorus were minor constituents of the coating (maps not shown). Figure 4(e) shows a scanning electron micrograph of the coating surface. The nodule sizes typically range from 20 to 40 μm. Deep cavities occur between the nodules. Individual nodules appear to consist of an agglomeration of finer nodules. EDX analysis in an area of 30 x 30 μm revealed (in at%) 72.0%O, 24.0% Si, 2.6% P, < 1%Nb, < 1% K, < 1% Na, suggesting that SiO₂ is the main constituent. SiO₂ is formed by thermolysis of silicate ions due to the high temperatures generated at the discharge sites.

Figure 5 shows scanning electron micrographs of the cross-section (Fig. 5 (a)) and the surface (Fig. 5 (b)) of the coating formed in the presence of 3 g l⁻¹ MgB₂ for 720 s with i_n/i_p of 1. The

coating thickness, about 65 μm , and nodular surface morphology are similar to those of the coating formed in the absence of MgB_2 . The nodular structure results in significant local variability in the thickness, with deep fissures between the nodules. Large cavities are present in the inner coating region, with sizes of up to several tens of microns. A thin layer of material, about 2 to 10 μm thick, containing small pores, extends along the niobium/coating interface. The inner layer material appears less porous than the foam-like material that constitutes the nodules in the outer coating regions. The layer also exhibits lighter regions in the backscattered micrograph of Fig. 5 (a), owing to the increased electron scattering from niobium-rich regions of coating material, which are interspersed with darker regions, presumed to be silicon-rich. The lighter regions probably contain Nb_2O_5 , which is shown to be present in the coating according to the later results of XRD. In particular, a relatively continuous barrier layer of niobium-rich oxide, about 1 μm thick, is located immediately adjacent to the niobium substrate (see inset in Fig. 5 (a)). Figure 5 (c) shows a higher magnification image of the coating surface revealing MgB_2 particles attached to the nodules and within the cavities between the nodules.

Figure 6(a) shows a backscattered electron micrograph of a cross-section of the coating formed in the presence of 8 g l^{-1} MgB_2 particles. From observations of several sections the coating was between 50 to 110 μm thick. The coating consisted of inner regions of more compact oxide of light appearance, and more foam-like, darker, oxide. Previous study showed that magnesium was mainly detected in the foam-like regions, which were relatively richer in silicon, while niobium was mainly present in the more compact oxide [1]. Closer examination showed that the majority of the pores contained micron- and sub-micron sized particles (Fig. 6(b) see arrows). The particles are of similar size to those of the as-received MgB_2 powder [1]. EDS point analysis of the particles revealed high concentrations of magnesium indicating the presence of MgB_2 .

Figure 6(c) shows the coating surface formed in the electrolyte containing 8 g l^{-1} MgB_2 . The coating also has a nodular surface, however, the nodules are less densely packed than in the absence of MgB_2 and a smoother porous material is visible between the nodules at the bottom of the interstices, as shown in Fig. 6(d). Large pores are evident of about 8 μm diameter and a region of finer pores of diameter in the approximate range 0.1 to 1 μm . It is known from previous work that formation of coatings in electrolytes containing added nanoparticles can reduce the porosity of coatings [41, 42], which may be due to their effect on the number and intensity of the microdischarges and hence, their influence on the local temperatures achieved

at the discharge sites in the coatings. The latter may affect both the chemical composition and the viscosity of the coating material, and hence the escape of oxygen, hydrogen and water vapour from the coating that can generate porosity [3]. Comparison of Figs 4 (e) and 5(c) that show the surfaces of coatings formed without and with MgB_2 respectively, suggests a lower porosity in the coating formed in the presence of MgB_2 . Furthermore, the voltage-time curves of Fig 1 (c) reveal a higher voltage with the presence of MgB_2 , which may be associated with a greater intensity of the discharges. The porosity is formed by escape of gas from molten or softened oxide. Cracks are also evident, which may be due to the stresses created when the coating material cools rapidly after discharge terminate. Such cracks are commonly encountered in PEO coatings. The surfaces of the interstitial coating material and the nodules are decorated by fine particles of ≈ 0.1 to $1 \mu\text{m}$ diameter, which is the size range of the MgB_2 powder. EDX analysis (at.%) of the coating surface in an area of $10 \times 20 \mu\text{m}$ revealed a Mg:Si ratio of 0.63, compared with 0.29 for the coating formed using 3 g l^{-1} MgB_2 , respectively. (Boron could not be analysed owing to the low energy of the characteristic X-rays). Thus, an increased concentration of MgB_2 in the electrolyte increased the incorporation of particles into the coating.

Results of XRD are shown in Fig. 7(a) for untreated niobium and following PEO at $i_n/i_p = -1$ for 720 s in MgB_2 -free electrolyte. A sharp peak due to Nb_2O_5 and a broad peak between $\sim 15^\circ$ to 30° due to amorphous material was present for the coated specimen. Owing to the coating thickness, no peaks were resolved from the substrate. Following PEO for 720 s in particle-containing electrolytes, peaks due to MgB_2 , Nb_2O_5 and amorphous material were present (Fig. 7(b)). The multiple peaks for 8 g l^{-1} MgB_2 compared with the single peak for 3 g l^{-1} MgB_2 indicated a greater presence of MgB_2 in the former specimen. No decomposition or oxidation products of MgB_2 were detected.

Incorporation of MgB_2 may follow migration of particles to the coating surface, dependent upon the zeta potential of the MgB_2 . Additionally, boiling and refluxing of the electrolyte in the pores and interstices of the coating surface may draw MgB_2 particles into the coating as the sites cool. MgB_2 may then deposit on the coating surfaces, adhering to the coating due to van de Waals or electrostatic forces, mechanical interlocking or chemical bonding. The particles would later be trapped within the coating by subsequent deposition of oxide as the coating grows.

3.5 Superconductivity measurements

The magnetisation has been measured as a function of the applied field (in the plane of the specimen) for four samples (uncoated niobium, PEO without MgB₂ and PEO with 3 and 8 g l⁻¹ of MgB₂) (Fig. 8), at 6 K, which is below the critical temperature of MgB₂ (about 39 K) and niobium (9.25 K). The initial magnetization curve for the uncoated niobium sample shows a behaviour which is expected. Flux starts to penetrate gradually at relatively low field caused by field enhancement at the edges of the rectangular sample. Strong pinning (hysteresis) and sudden flux release are observed in the hysteresis loop. PEO with no MgB₂ changes that behaviour. Some flux is already released at H=0. As PEO only affects the surface of the material this indicates that the pinning behaviour observed without PEO is a surface effect. PEO with MgB₂ yields a more gradual flux release than uncoated niobium and PEO without MgB₂.

Figure 9 shows the magnetic moment divided by the applied field M/H normalized to unity as a function of applied field for the initial magnetization curve. In this plot a value of M/H=1 signifies the full sample in a flux free Meissner state. While the magnetic moment itself is an extensive property this normalized curve allows a better comparison of the four samples. As all four curves look very similar one can conclude that the PEO has no influence on the initial magnetization curve. The complete behaviour is dominated by the niobium substrate, which accounts for the major part of the superconducting material. Note that the PEO coating containing the MgB₂ particles is only about 50-100 μm thick compared to the niobium substrate of 2 mm thickness.

In order to probe superconductivity of the MgB₂ coating the 8 g l⁻¹ sample, which has the higher amount of MgB₂ in the coating, has been measured at several temperatures above the critical temperature of niobium (9.25 K) (Fig. 10). For all temperatures, the dominating effect is the paramagnetism of niobium as the resulting magnetic moment is orientated in the same direction as the applied field. The measured moment is slightly larger than expected for a pure 0.1988g niobium sample with a magnetic susceptibility of $X=217\mu\text{emu/mole}$ [43]. This can be explained by competing diamagnetism of SiO₂ and Nb₂O₅.

The superconductivity of MgB₂ is visible though by the hysteresis and the initial magnetization curve alike. For the initial curve, if measured above the critical temperature of MgB₂ (about 39

K), there is a linear correlation between magnetization and applied field indicative of paramagnetic behaviour. If however, the temperature is below 42 K the initial slope M/H is weaker indicating additional diamagnetic behaviour of the superconducting MgB_2 . The trend for the temperatures of 12, 25 and 35 K is consistent with this interpretation. The closer the temperature is to the critical temperature of MgB_2 the earlier the flux penetration occurs. The hysteresis loop shows for lower temperatures a larger $\Delta M (H=0)$. This can be interpreted as stronger flux pinning for lower temperatures as expected for a superconductor. Hysteresis remains beyond 45 K where it cannot be attributed to pinning in a superconductor. At this temperature there is no sign of diamagnetism left further ruling out superconductivity. The magnetization curves at 45 and 300 K are therefore consistent with a weak ferromagnet with a Curie temperature above 300 K. Note that MgB_2 exhibits ferromagnetic behaviour in the normal conducting state [44].

4. Conclusions

1. Silicon-rich PEO coatings formed on niobium under the present conditions grow at a constant rate in the first 720 s of the process. Thereafter, the rate falls steeply due to large reductions and fluctuations in voltage and intermittent sparking.
2. MgB_2 particles are readily incorporated into the coating, with incorporation increased by increasing the MgB_2 content of the electrolyte from 3 to 8 g l⁻¹.
3. The superconductivity of the incorporated MgB_2 , probed with squid magnetometry, disclosed flux pinning and diamagnetic behaviour, both indicative of a superconducting state.

Acknowledgements

The authors acknowledge funding from the European Union's Horizon 2020 research and innovation programme under the Marie Skłodowska-Curie grant agreement No. 665593 awarded to UKRI Science and Technology Facilities Council (STFC). They also are grateful to the Material Characterisation Laboratory at ISIS, STFC Rutherford Appleton Laboratory for superconductivity measurements.

References

- [1] S. Aliasghari, P. Skeldon, X. Zhou, R. Valizadeh, T. Junginger, G.B.G. Stenning, G. Burt, Communication - Formation of a superconducting MgB₂-containing coating on niobium by plasma electrolytic oxidation, *ECS J. Solid State Sci. Technol.* 8 (2019) N39-N41.
- [2] A.L. Yerokhin, X. Nie, A. Leyland, A. Matthews, S.J. Dowey, Plasma electrolysis for surface engineering, *Surf. Coat. Technol.* 122 (1999) 73–93.
- [3] T.W. Clyne, S.C. Troughton, A review of recent work on discharge characteristics during plasma electrolytic oxidation of various metals, *Internat. Mater. Rev.* 64 (2019) 127-162.
- [4] J.A. Curran, T.W. Clyne, Porosity in plasma electrolytic oxidation coatings, *Acta Mater.* 54 (2006) 1985-1993.
- [5] X. Zhang, S. Aliasghari, A. Nemcova, T.L. Burnett, I. Kubena, M. Smid, G.E. Thompson, P. Skeldon, P.J. Withers, X-ray computed tomographic investigation of the porosity and morphology of plasma electrolytic oxidation coatings, *ACS Appl. Mater. Inter.* 8 (2016) 8801-8810.
- [6] C.S. Dunleavy, I.O. Golosny, J.A. Curran, T.W. Clyne, Characterisation of discharge events during plasma electrolytic oxidation, *Surf. Coat. Technol.* 203 (2009) 3410-3419.
- [7] A. Nomine, S.C. Troughton, A.V. Nomine, G. Henrion, T.W. Clyne, High speed video evidence of localised discharge cascades during plasma electrolytic oxidation, *Surf. Coat. Technol.* 269 (2015) 125-130.
- [8] S.C. Troughton, A. Nomine, A.V. Nomine, G. Henrion, T.W. Clyne, Synchronised electrical monitoring and high speed video of bubble growth associated with individual discharges during plasma electrolytic oxidation, *Appl. Surf. Sci.* 359 (2015) 405-411.
- [9] F. Monfort, A. Berkani, RE. Matykina, P. Skeldon, G.E. Thompson, H. Habazaki, K. Shimizu, Development of anodic coatings on aluminium under sparking conditions in silicate electrolyte, *Corros. Sci.* 49 (2007) 672-693.

- [10] A. Apelfeld, B. Krit, V. Ludin, N. Morozova, B. Vladimirov, R. Z. Wu, The characterization of plasma electrolytic coatings on AZ41 magnesium alloy. *Surf. Coat. Technol.* 322 (2017) 127-133.
- [11] M. Laveissière, H. Cerda, J. Roche, L. Cassayre, L. Arurault, In-depth study of the influence of electrolyte composition on coatings prepared by plasma electrolytic oxidation of TA6V alloy, *Surf. Coat. Technol.* 361 (2019) 50-62.
- [12] E. Matykina, R. Arrabal, F. Monfort, P. Skeldon, G.E. Thompson, Incorporation of zirconia into coatings formed by DC plasma electrolytic oxidation of aluminium in nanoparticle suspensions, *Appl. Surf. Sci.* 255 (2008) 2830-2839.
- [13] Bih-Show Lou, Yi-Yuan Lin, Chuan-Ming Tseng, Yu-Chu Lu, Jenq-Gong Du, Jyh-Wei Lee, Plasma electrolytic oxidation coatings on AZ31 magnesium alloys with Si_3N_4 nanoparticle additives, *Surf. Coat. Technol.* 332 (2017) 358-367.
- [14] A. V. Apelfeld, A. A. Ashmarin, A. M. Borisov, A. V. Vinogradov, S. V. Savushkina E. A. Shmytkova, Formation of zirconia tetragonal phase by plasma electrolytic oxidation of zirconium alloy in electrolyte comprising additives of yttria nanopowder, *Surf. Coat. Technol.* 328 (2017) 513-517.
- [15] G. Sundararajan, L. Rama Krishna, Mechanisms underlying the formation of thick alumina coatings through MAO coating technology, *Surf. Coat. Technol.* 167 (2003) 269-277.
- [16] L.O. Snizhko, A.L. Yerokhin, N.L. Gurevina, V.A. Patalakha, A. Matthews, Excessive oxygen evolution during plasma electrolytic oxidation of aluminium, *Thin Solid Films* 56 (2007) 460-464.
- [17] H. Padamsee, The science and technology of superconducting cavities for accelerators, *Supercond. Sci. Technol.* 14 (2001) R28.

- [18] S. Casalbuoni, E.A. Knabbe, J. Kötzler, L. Lilje, L. Von Sawilski, P. Schmueser, B. Steffen, Surface superconductivity in niobium for superconducting RF cavities, *Nuclear Instrum. Meth. A* 538 (2005) 45-64.
- [19] M. Sowa, A. Kazek-Kęsik, A. Krzakała, R. P. Socha, G. Dercz, J. Michalska, W. Simka, Modification of niobium surfaces using plasma electrolytic oxidation in silicate solutions, *J. Solid State Electr.* 18 (2014) 3129-3142.
- [20] S. Stojadinović, R. Vasilić, Orange–red photoluminescence of $\text{Nb}_2\text{O}_5:\text{Eu}^{3+}$, Sm^{3+} coatings formed by plasma electrolytic oxidation of niobium, *J. Alloy. Compd.* 685 (2016) 881-889.
- [21] J. Nagamatsu, N. Nakagawa, T. Muranaka, Y. Zenitani, J. Akimitsu, Superconductivity at 39 K in magnesium diboride, *Nature* 410 (2001) 63-64.
- [22] D. Mijatovic, A. Brinkman, J.W.M. Hilgenkamp, H. Rogalla, A.J.H.M. Rijnders, D.H.A. Blank, Pulsed-laser deposition of MgB_2 and B thin films, *Appl. Phys. A: Mater. Sci. Proc.* 79 (2004) 1243-1246.
- [23] S. Zhang, C.-Y. Deng, X. Wang, Y.-P. Wu, Y. Fu, and X.-H. Fu, Superconducting MgB_2 film prepared by chemical vapor deposition at atmospheric pressure of N_2 , *Thin Solid Films* 584 (2015) 300-304.
- [24] K. Ueda, M. Naito, As-grown superconducting MgB_2 thin films prepared by molecular beam epitaxy, *Appl. Phys. Lett.* 79 (2001) 2046-2048.
- [25] X.X. Xi, A.V. Pogrebnyakov, S.Y. Xu, K. Chen, Y. Cui, E.C. Maertz, C.G. Zhuang, Qi Li, D.R. Lamborn, Joan Marie Redwing, Zi-kui Liu, A. Soukiassian, D.G. Schlom, X.J. Weng, E.C. Dickey, Y.B. Chen, W. Tian, X.Q. Pan, S.A. Cybart, R.C. Dynes, MgB_2 thin films by hybrid physical-chemical vapor deposition, *Physica C: Superconductivity* 456 (2007) 22-37.
- [26] B.H. Moeckly, W.S. Ruby, Growth of high-quality large-area MgB_2 thin films by reactive evaporation, *Supercond. Sci. Technol.* 19 (2006) L21-L24.

- [27] K.S. Vijayaragavan, S.K. Putatunda, A. Dixit, G. Lawes, Electroless deposition of superconducting MgB₂ films on various substrates, *Thin Solid Films* 51 (2010) 658-661.
- [28] A.B. Jadhav, S.H. Pawar, Electrochemical synthesis of superconducting magnesium diboride films: a novel potential technique, *Supercond. Sci. Technol.* 16 (2003) 752-759.
- [29] M. Ochsenkühn-Petropoulou, .L. Mendrinou, A. Altzoumailis, and R. Argyropoulou, Production and characterization of MgB₂ coatings on various substrates by electrophoretic deposition, *J. Mater. Processing Technol.* 161 (2005) 16-21.
- [30] M. Nath and B.A. Parkinson, A simple sol-gel synthesis of superconducting MgB₂ nanowires, *Adv. Mater.* 18 (2006) 1865-1868.
- [31] N. Peng, G. Shao, C. Jeynes, R. P. Webb, R. M. Gwilliam, G. Boudreault, D. M. Astill, and W. Y. Liang, Ion beam synthesis of superconducting MgB₂ thin films, *Appl. Phys. Lett.* 82 (2003) 236-238.
- [32] H. Padamsee, The science and technology of superconducting cavities for accelerators *Supercond. Sci. Technol.* 14 (2001) R28.
- [33] S. Casalbuoni, E. A. Knabbe, J. Kötzler, L. Lilje, L. Von Sawilski, P. Schmueser, B. Steffen, *Nuclear Instrum. Meth. A*, 538 (2005) 45-64.
- [34] S. Aliasghari, P. Skeldon, G.E. Thompson, Plasma electrolytic oxidation of titanium in a phosphate/silicate electrolyte and tribological performance of the coatings. *App. Surf. Sci.* 316 (2014) 463-476.
- [35] L. Young, F.G.R. Zobel, An ellipsometric study of steady-state high field ionic conduction in anodic oxide films on tantalum, niobium, and silicon, *J. Electrochem. Soc.* 113 (1966) 277-283.
- [36] H. Habazaki, T. Ogasawara, H. Konno, K. Skimizu, K. Asami, K. Saito, P. Skeldon, G.E. Thompson, Growth of anodic oxide films on oxygen-containing niobium, *Electrochim. Acta* 50 (2005) 5334-5339.

[37] F. Jaspard-Mécuson, T. Czerwiec, G. Henrion, T. Belmonte, L. Dujardin, A. Viola, J. Beauvoir, Tailored aluminium oxide layers by bipolar current adjustment in the Plasma Electrolytic Oxidation (PEO) process, *Surf. Coat. Technol.* 2012 (2007) 8677-8682.

[38] Aleksey Rogov, Aleksey Yerokhin, Allan Matthews, The role of cathodic current in plasma electrolytic oxidation of aluminum: Phenomenological concepts of the “soft sparking” mode, *Langmuir* 33 (2017) 11059-11069.

[39] A.B.Rogov, V.R.Shayapov, The role of cathodic current in PEO of aluminum: Influence of cationic electrolyte composition on the transient current-voltage curves and the discharges optical emission spectra, *Appl. Surf. Sci.* 394 (2017) 323-332.

[40] R.Arrabal, E.Matykina, T.Hashimoto, P.Skeldon, G.E.Thompson, Characterization of AC PEO coatings on magnesium alloys, *Surf. Coat. Technol.* 203 (2009) 2207-2220.

[41] Baojun Han, Yang Yang, Hao Deng, Yaowu Chen, Chubin Yang, Plasma-electrolytic-oxidation coating containing Y_2O_3 nanoparticles on AZ91 magnesium alloy, *Int. J. Electrochem. Sci.*, 13 (2018) 5681-5697.

[42] S.V. Gnedenkov, S.L. Sinebryukhov, D.V. Mashtalyar, I.M. Imshinetskiy, A.V. Samokhin, Yu. V. Tsvetkov, Fabrication of coatings on the surface of magnesium alloy by plasma electrolytic oxidation using ZrO_2 and SiO_2 nanoparticles, *J. Nanomater.* 2015 (2015) Article ID 154298, 12 pages.

[43] E.W. Collings, R.D. Smith, The magnetic susceptibility of niobium, *J. Less-Comm. Met.*, 27 (1972) 389-401.

[44] S. Reich, G. Leitus, I. Felner, On the magnetism of the normal state in MgB_2 , *J. Supercond.* 15 (2002) 109-111.

Figure captions:

Figure 1. Voltage-time curves during PEO of niobium at 500 mA cm^{-2} in silicate-phosphate electrolyte with a frequency of 50 Hz and duty cycle of 50%; (a) 2000 s, i_n/i_p -1; (b) 720 s, i_n/i_p in the range of -1 to -1.27; (c) 720 s, i_n/i_p and 3 and 8 g l^{-1} MgB_2 in the electrolyte.

Figure 2. Optical emission spectra recorded during PEO of niobium in silicate-phosphate electrolyte (500 mA cm^{-2} , 50 Hz, a duty cycle of 50%, i_n/i_p -1).

Figure 3. Coating thickness-time relationship for PEO of niobium in silicate-phosphate electrolyte (500 mA cm^{-2} , 50 Hz, a duty cycle of 50%, i_n/i_p -1). The thickness was measured by SEM of coating cross-sections.

Figure 4. (a) Scanning electron micrograph (secondary electrons) of the coating cross-section following PEO of niobium for 720 s in silicate-phosphate electrolyte (500 mA cm^{-2} , 50 Hz, a duty cycle of 50%, i_n/i_p -1); (b-d) EDS elemental maps of niobium, silicon, oxygen, phosphorus. (e) Coating surface.

Figure 5. Scanning electron micrographs of (a) the coating cross-section (backscattered electrons) and (b, c) the coating surface (secondary electrons) following PEO of niobium for 720 s in silicate-phosphate electrolyte containing 3 g l^{-1} MgB_2 (500 mA cm^{-2} , 50 Hz, a duty cycle of 50%, i_n/i_p -1).

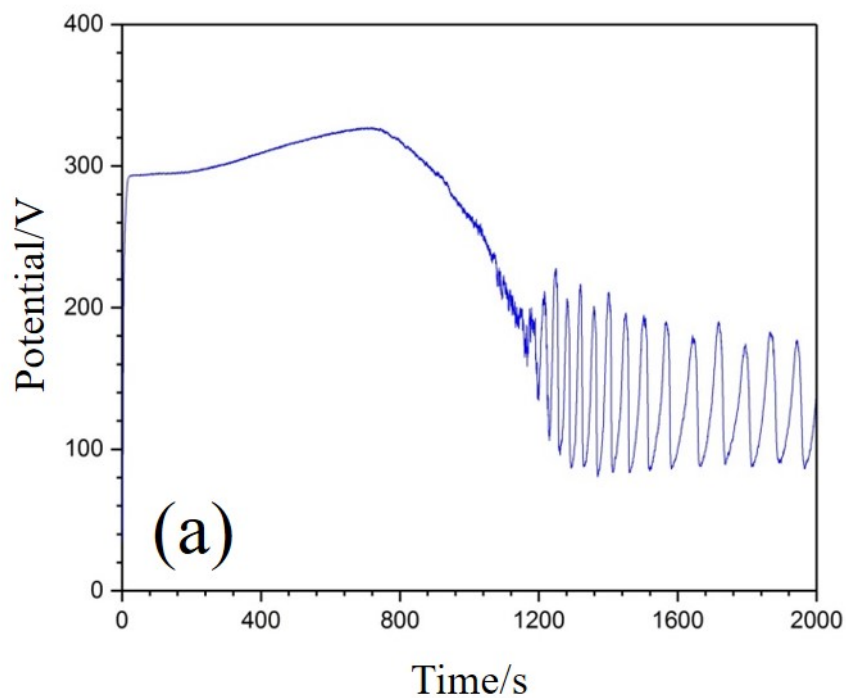
Figure 6. Scanning electron micrographs of (a, b) the coating cross-section (backscattered electrons) and (c, d) the coating surface (secondary electrons) following PEO of niobium for 720 s in silicate-phosphate electrolyte containing 8 g l^{-1} MgB_2 (500 mA cm^{-2} , 50 Hz, a duty cycle of 50%, i_n/i_p -1).

Figure 7. XRD patterns for niobium (a) before and following PEO for 720 s in silicate-phosphate electrolyte (500 mA cm^{-2} , 50 Hz, a duty cycle of 50%, i_n/i_p -1). (b) Following 720 s in electrolytes containing 3 and 8 g l^{-1} MgB_2 .

Figure 8. Magnetic moment as a function applied field measured with a squid magnetometer at 6 K for niobium in the uncoated condition, following PEO in MgB₂-free electrolyte and following PEO in electrolyte containing 3 and 8 g l⁻¹ MgB₂.

Figure 9. Magnetic moment divided by applied field normalized to its maximum value as a function of applied field at 6 K for niobium in the uncoated condition, following PEO in MgB₂-free electrolyte and following PEO in electrolyte containing 3 and 8 g l⁻¹ MgB₂. A value of 1 indicates the entire sample being in a flux free Meissner state.

Figure 10. Magnetic moment as a function applied field at temperatures from 12 to 300 K for niobium following PEO in electrolyte containing 8 g l⁻¹ MgB₂. The effect of the MgB₂-containing coating on the initial magnetization curve is clearly visible in the inset.



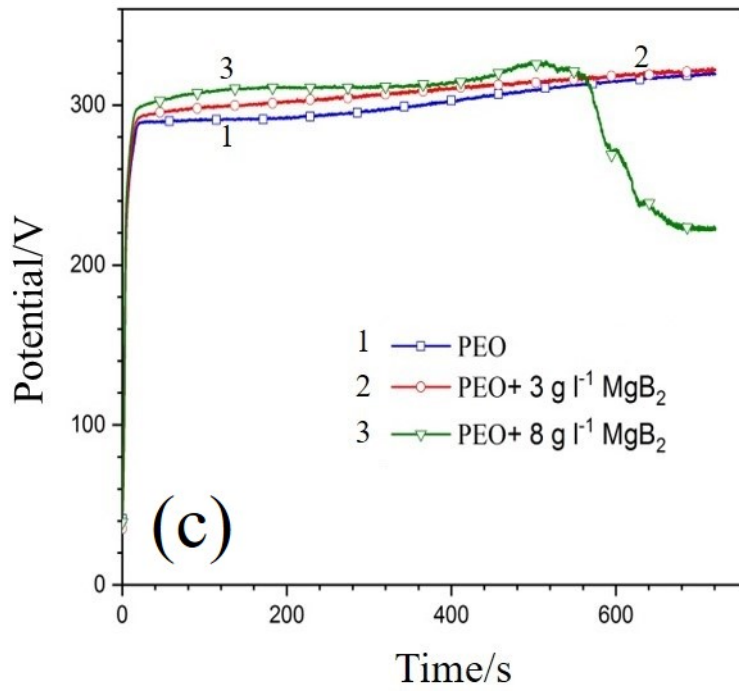
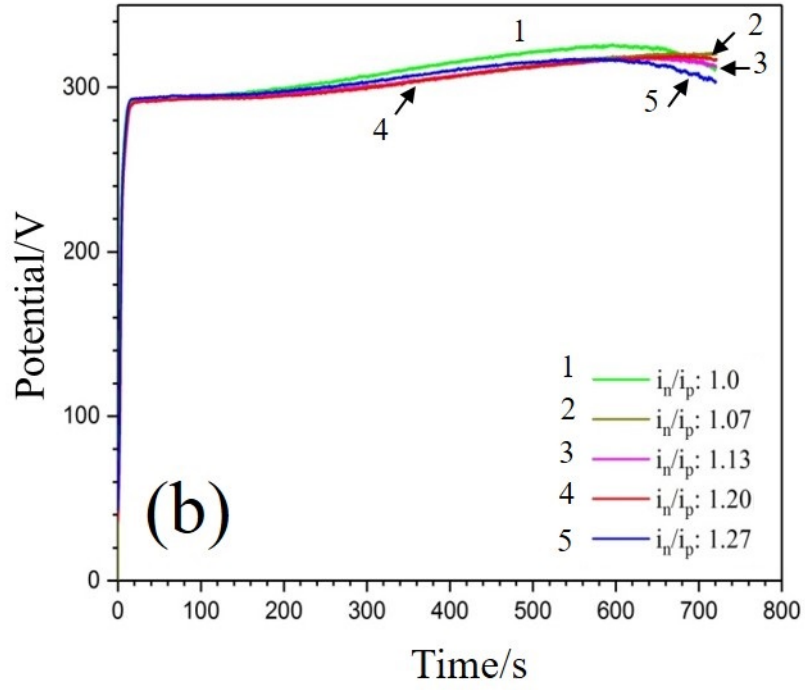


Figure 1.

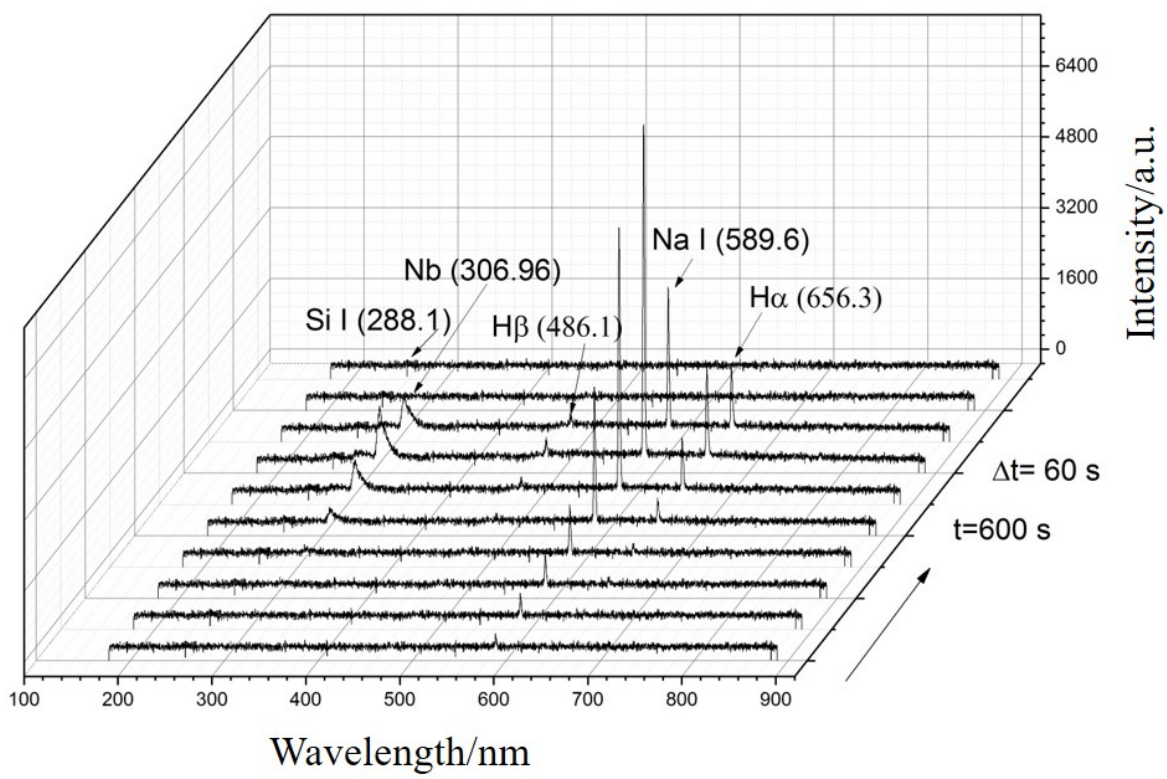


Figure 2.

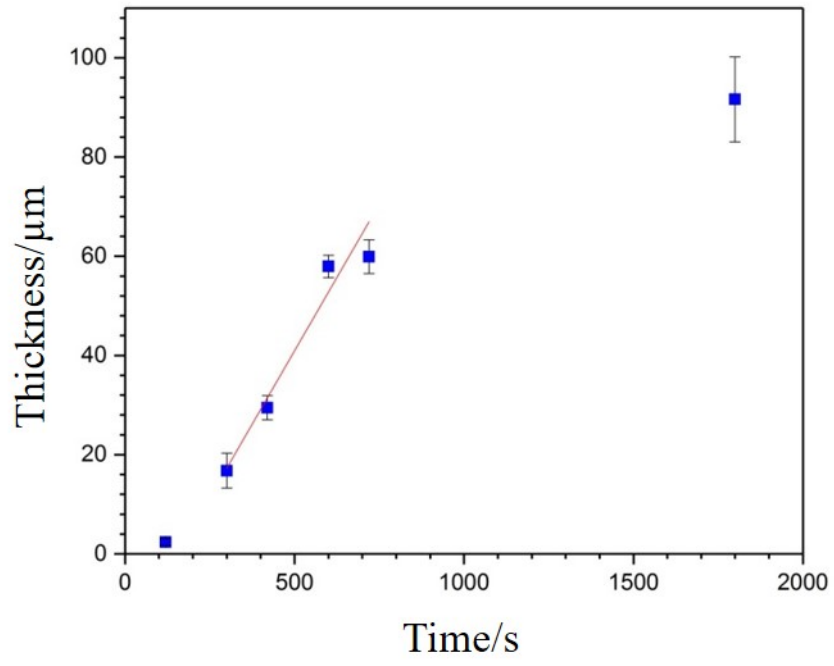


Figure 3.

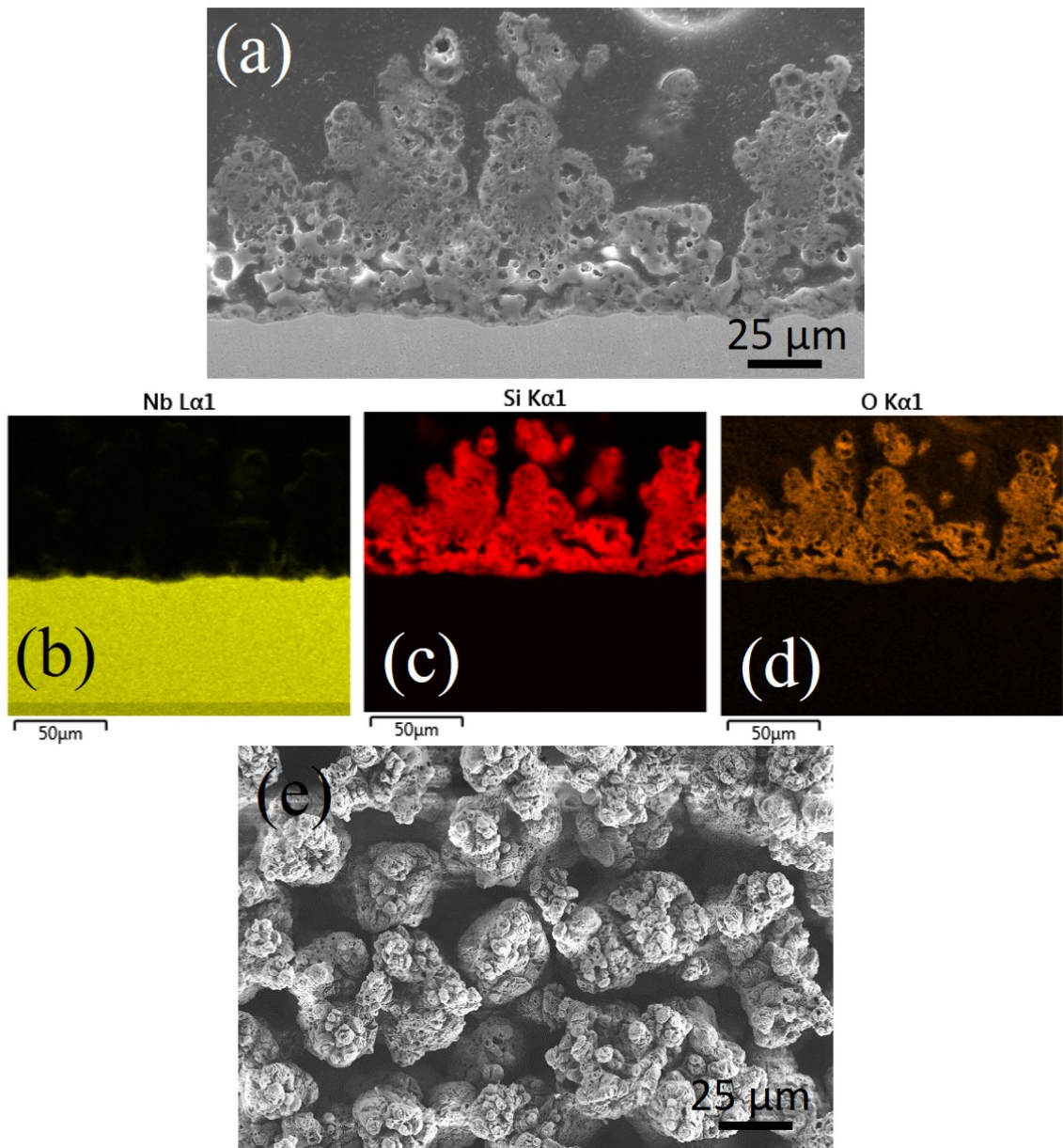


Figure 4.

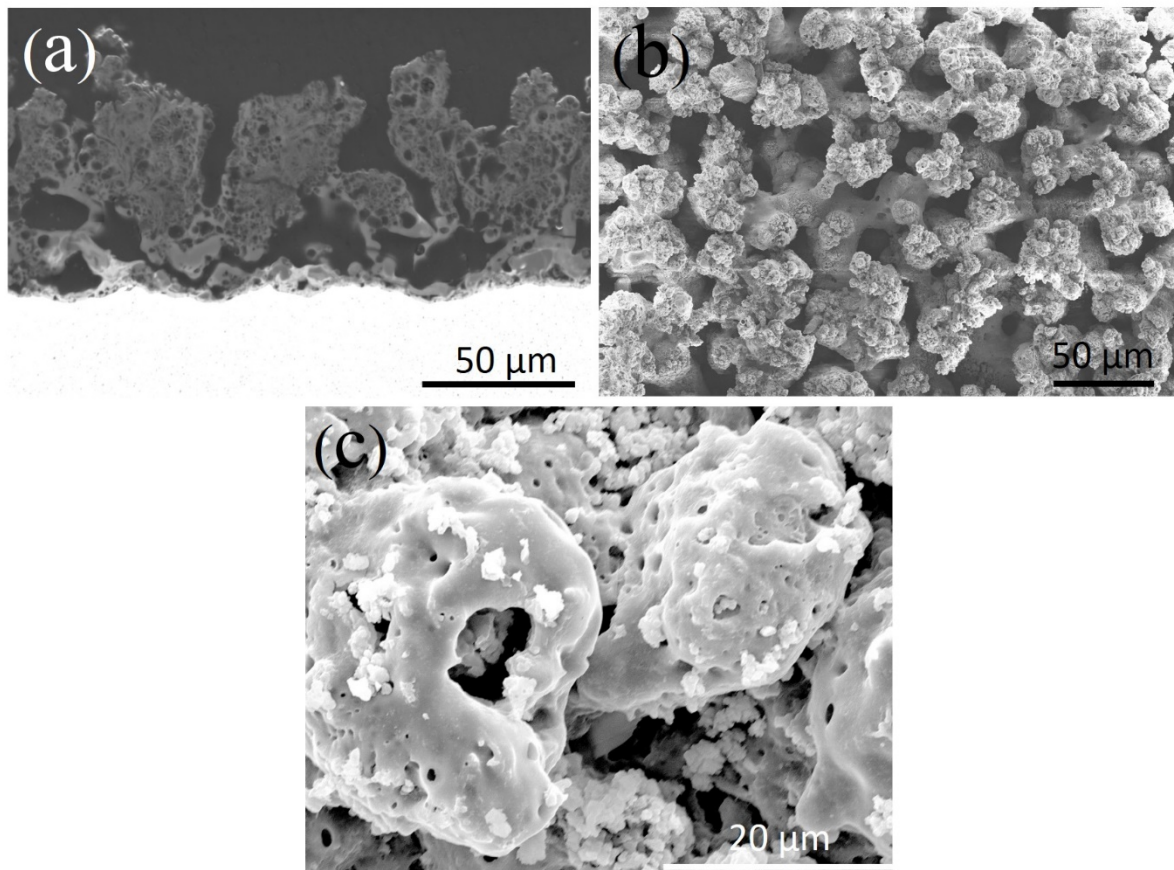


Figure 5.

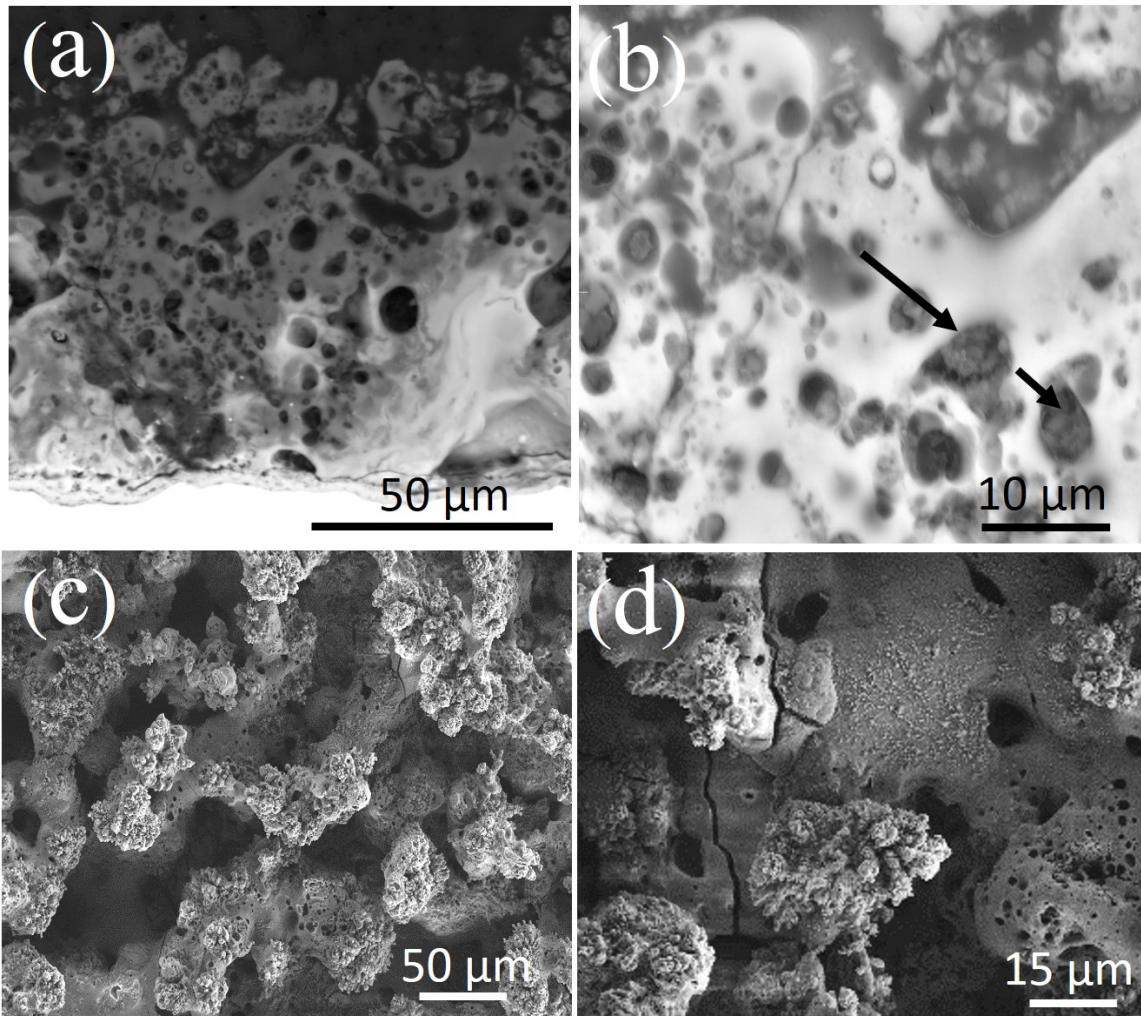


Figure 6.

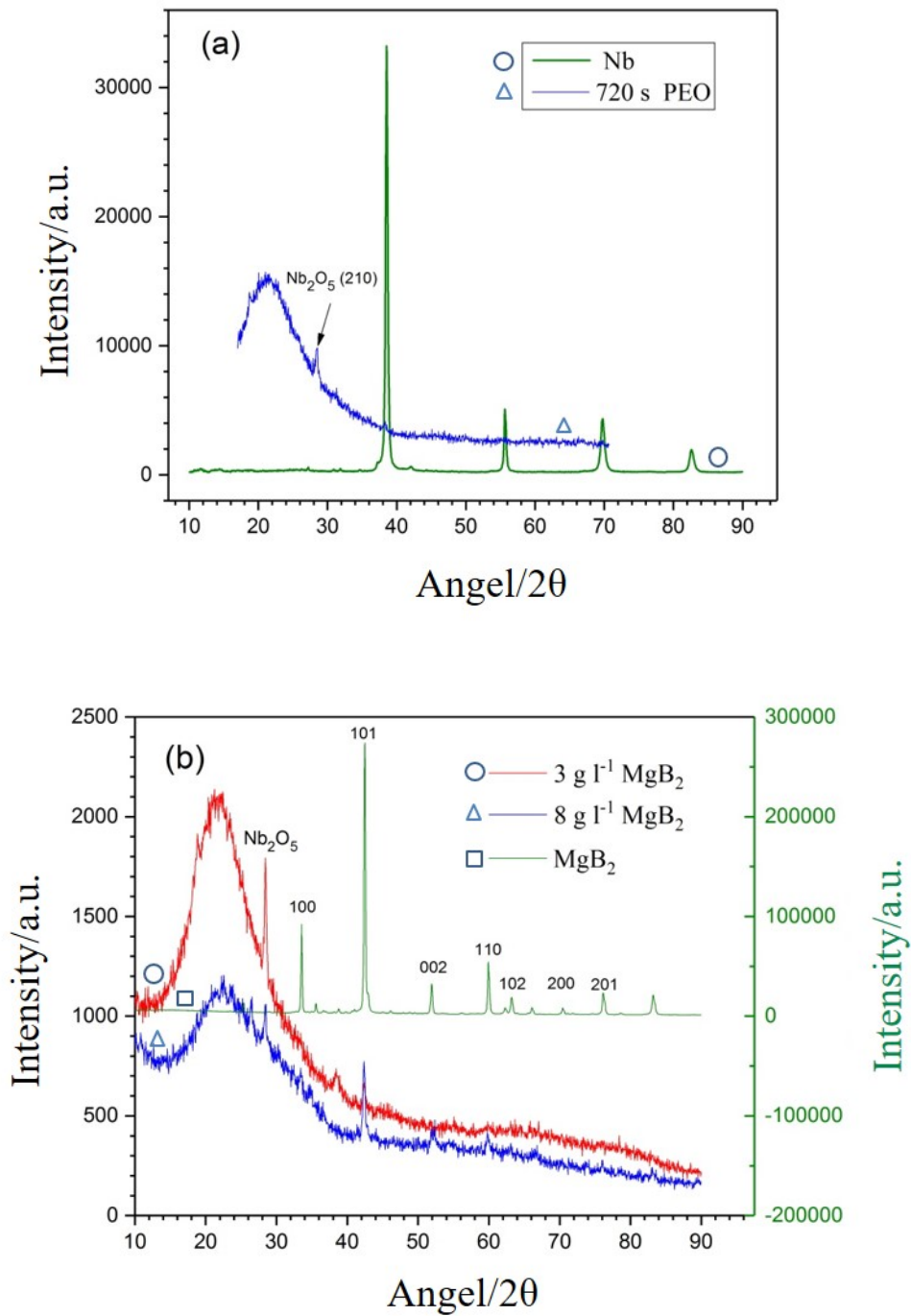


Figure 7.

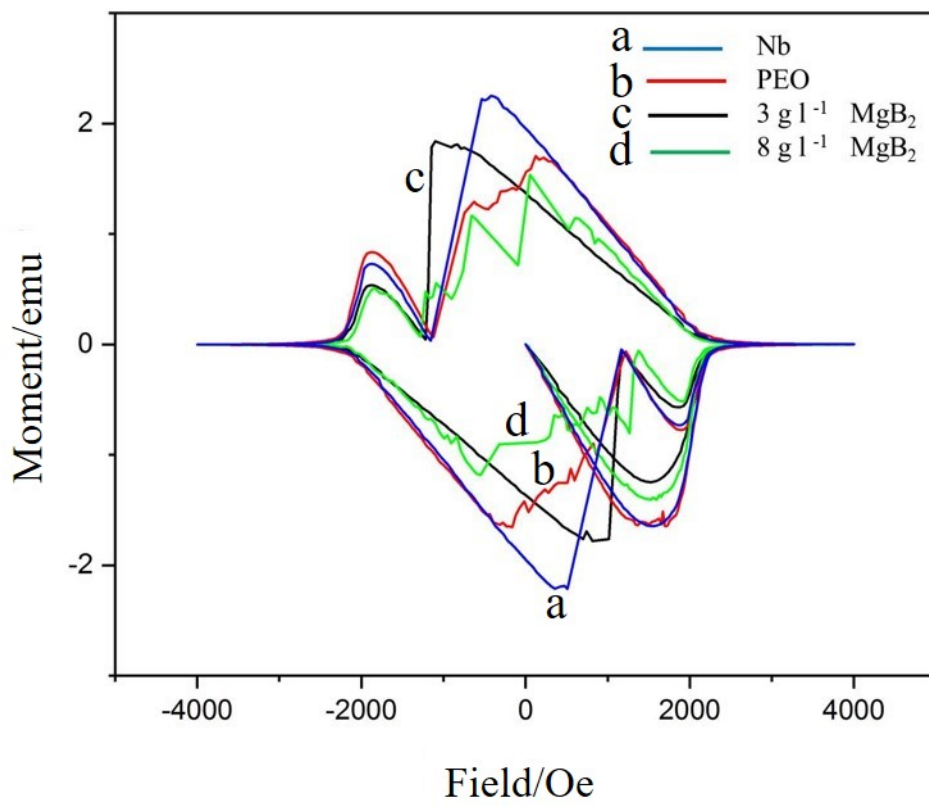


Figure 8.

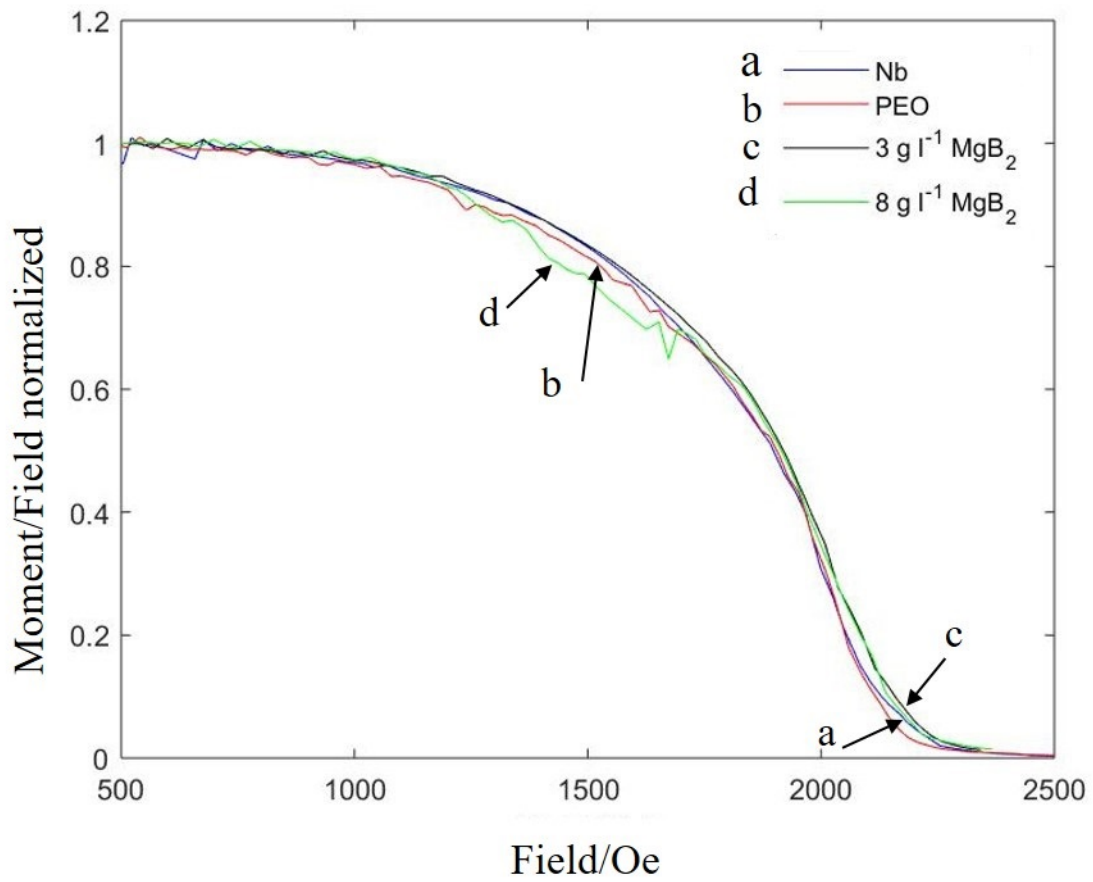


Figure 9.

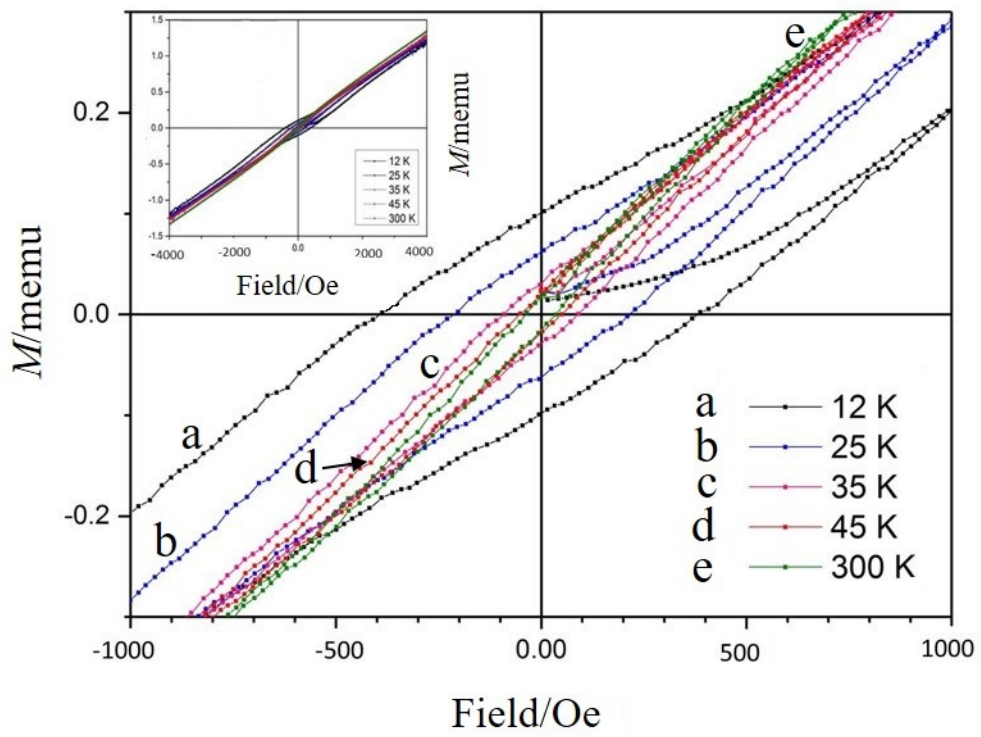


Figure 10.